Pergamon

Int. J. Solids Structures Vol. 32, No. 15, pp. 2127–2154, 1995

0020-7683/95 $9.50 + .00

0020-7683(94)00254-1

THE STRESS FIELD IN A CRACKED BRITTLE MATRIX COMPOSITE CYLINDER WITH A FRICTIONAL INTERFACE

AUTAR K. KAW, SENTHIL KUNCHITHAPATHAM
Mechanical Engineering Department, University of South Florida, Tampa, FL 33620-5350, U.S.A.

and

NICHOLAS J. PAGANO
Materials Directorate, WL/MLBM, WPAFB, OH 45433-6533, U.S.A.

(*Received* 26 *February* 1994; *in revised form* 10 *October* 1994)

Abstract—The effect of a frictional interface on the response of a unidirectional ceramic matrix composite under a remote axial tensile strain and a temperature change is studied. The geometry of the composite is approximated by a concentric cylinder model with an annular crack in the axial plane of the matrix. The fiber–matrix interface follows the Coulomb friction law. On applying the boundary and the interface continuity conditions, the solution is obtained in terms of coupled integral equations and inequality conditions.

The extent of the interfacial damage and the stress fields in the fiber and the matrix along the interface are studied for a SiC/CAS composite system as a function of the coefficient of friction, temperature change, and remote uniform axial strain. These results are also compared with a shear lag analysis model for an identical geometry and loading.

INTRODUCTION

Ceramic matrix composites are becoming attractive as load bearing structures for high temperature and corrosive atmosphere applications. Although these composites have higher ultimate strength and strain than monolithic ceramics, matrix cracking followed by interfacial failure is still a critical issue in their use.

Consider a unidirectional ceramic composite subjected to an axial strain along the fiber direction. The cracks will first develop in the matrix owing to its lower failure strain than that of the fiber. When a matrix crack reaches the interface of the fiber and the matrix, the interface may open or slip. This opening/slipping of the interface blunts the crack and slows and arrests the propagation of the crack. Although this blunting of the crack increases the fracture toughness of the composite, the damage in the interface reduces the axial compressive and transverse strength of the composite (Steif, 1984). Because of these conflicting effects of interfacial damage, it becomes important to understand fully the mechanics of matrix fracture in ceramic matrix composites as a function of material, geometrical, and loading parameters.

Axisymmetric three-dimensional failure mechanics models, which account for all equations of elasticity as well as assuming an imperfect interface, for the fracture in ceramic matrix composites are reported in the literature. These include the work of Schweitert and Steif (1991), Wijeyewickrema and Keer (1993), and Kaw and Pagano (1993). The interface in all the above three studies is modeled differently.

Wijeyewickrema and Keer (1993) solved the problem of a composite cylinder made of a solid cylinder (fiber) bonded to a surrounding hollow cylinder (matrix) of finite outer radius. An annular crack was assumed in the matrix. The composite cylinder was subjected to a remote uniform tensile strain. The interface included a slip zone and was assumed to have a constant shear stress equal to the shear strength of the interface. This is a reasonable assumption when the interfacial friction coefficient is small (Aksel *et al.*, 1991).

Kaw and Pagano (1993) solved for the same composite geometry as Wijeyewickrema and Keer (1993). Kaw and Pagano (1993) included an imperfect interface in the composite cylinder model but by approximating the interface by distributed shear springs of constant stiffness. Their model included also the effects of temperature change.

Schweitert and Steif (1991) used a similar geometry to the above two studies except for two differences. First, the outer radius of the matrix was assumed to be infinite. Second, a penny-shaped crack was assumed in the fiber (solid cylinder) instead of the annular crack in the matrix (hollow cylinder). The authors approximated the interface by the Coulomb friction law. The composite geometry was subjected to a pressure on the crack surface and a constant remote compressive radial stress. The pressure on the crack surface indirectly represented the matrix axial stresses due to a remote uniform axial strain. The remote radial stress indirectly represented residual stresses due to the mismatch of the linear coefficients of the thermal expansion coefficient and the Poisson's ratio of the fiber and the matrix.

In the present study, several assumptions made in Schweitert and Steif's (1991) model are relaxed as follows.

- The dilute fiber volume fraction assumption is replaced by a non-dilute fiber volume fraction.
- The fiber crack is replaced by an annular matrix crack. Furthermore, the annular crack does not necessarily have to be a through crack. It can be internal, edge, and/or touching the interface.
- The stresses due to the thermal expansion mismatch of the fiber and the matrix can be directly accounted for in the model.

These relaxed assumptions allow direct study of the combined effect of material, thermomechanical loading, and geometrical parameters. In the sections to follow is the formulation of the model. The effects of the coefficient of friction at the fiber–matrix interface and the linear coefficients of thermal expansion of the fiber–matrix on the extent of interfacial damage and the stress distribution at the interface under a thermomechanical load are studied. These results are compared with an approximate model for an identical geometry and loading. The approximate model is based on axial stresses being independent of the radial co-ordinate similar to Gu and Mangonon's (1992) radially constrained matrix model.

METHOD OF ANALYSIS

Geometry

The geometry of the composite cylinder consists of an infinitely long fiber bonded to an annular matrix of finite outer radius (Fig. 1). This concentric cylinder configuration can be viewed as an approximation for the representative volume element of a unidirectional composite reinforced by a hexagonal array of fibers. Following the work of Pagano and Brown (1993), one may also consider embedding this damaged concentric cylinder in a region that preserves the effective moduli of the uncracked material. In this manner, one may estimate the effect of the initial damage in a local region of the composite.

The cylindrical coordinates are denoted by r, θ, and z, and u_r and u_z are the radial and axial displacements, respectively. The radial, axial, hoop, and shear stresses are denoted by σ_{rr}, σ_{zz}, $\sigma_{\theta\theta}$, and σ_{rz}, respectively. The indices 0 and 1 stand for the fiber and the matrix, respectively.

The fiber is approximated by a linearly elastic, isotropic, homogeneous, and infinitely long solid cylinder of radius a, shear modulus μ_0, Poisson's ratio v_0, Young's modulus $E_0 = 2(1+v_0)\mu_0$, and linear coefficient of thermal expansion α_0. The matrix is approximated by a linearly elastic, isotropic, homogeneous, and infinitely long annular cylinder of inner radius a and outer radius c, shear modulus μ_1, Poisson's ratio v_1, Young's modulus, $E_1 = 2(1+v_1)\mu_1$, and linear coefficient of thermal expansion, α_1. An annular crack of length e−d ($a \leqslant d < e \leqslant c$) in the $z = 0$ plane, at a distance of $d-a$ from the interface is assumed in the matrix. The fiber volume fraction is $V_f = a^2/c^2$.

Boundary and continuity conditions

The composite cylinder is subjected to a monotonically increasing axial remote strain, ε_0, on the ends plus a constant temperature change, ΔT.

The imperfect interface between the fiber and the matrix follows the Coulomb friction law and may have open, slip, and stick zones.

The length of the open zone is z_1, and the length of the slip zone is $z_2 - z_1$. The kinetic and static coefficients of friction are considered to be equal. The friction coefficient ρ is assumed to be constant in the slip zone. The superscripts 0 and 1 denote the fiber and the matrix, respectively. The traction continuity conditions at the interface between the fiber and the matrix at $r = a$ are hence given by:

$$\sigma_{rr}^0(a, z) = \sigma_{rr}^1(a, z), \quad 0 \leqslant |z| < \infty, \tag{1a}$$

$$\sigma_{rz}^0(a, z) = \sigma_{rz}^1(a, z), \quad 0 \leqslant |z| < \infty. \tag{1b}$$

Furthermore, at the interface ($r = a$) between the fiber and the matrix, the zones are governed by the following.

Open zone

The crack surfaces are traction-free as given by

$$\sigma_{rz}^0(a, z) = 0, \quad 0 \leqslant |z| \leqslant z_1, \tag{2a}$$

$$\sigma_{rr}^0(a, z) = 0, \quad 0 \leqslant |z| \leqslant z_1, \tag{2b}$$

constrained by the crack-opening condition

$$u_r^1(a, z) - u_r^0(a, z) > 0, \quad 0 \leqslant |z| \leqslant z_1. \tag{2c}$$

Slip zone

Radial contact is maintained:

$$u_r^0(a, z) = u_r^1(a, z), \quad z_1 \leqslant |z| \leqslant z_2, \tag{2d}$$

and the shear stress is related to the radial stress through the coefficient of friction ρ:

$$\sigma_{rz}^0(a, z) = -\rho\, \sigma_{rr}^0(a, z), \quad z_1 \leqslant |z| \leqslant z_2. \tag{2e}$$

There needs to be a positive dissipation of energy in the slip zone implying the direction of the shear stress and increment in axial slip as

$$\operatorname{sgn}\left(\frac{\mathrm{d}}{\mathrm{d}t}[u_z^1(a, z) - u_z^0(a, z)]\right) = \operatorname{sgn}[\sigma_{rz}^0(a, z)], \quad z_1 \leqslant |z| \leqslant z_2. \tag{2f}$$

The variable t is a time-like parameter and is assumed to increase monotonically with increasing remote axial strain, ε_0. The constraining conditions include one that the radial stress is compressive:

$$\sigma_{rr}^0(a, z) < 0, \quad z_1 < |z| < z_2. \tag{2g}$$

Stick zone

The radial and axial displacements are continuous at the interface

$$u_r^0(a,z) = u_r^1(a,z), \quad z_2 \leqslant |z| < \infty, \tag{2h}$$

$$u_z^0(a,z) = u_z^1(a,z), \quad z_2 \leqslant |z| < \infty, \tag{2i}$$

constrained by a compressive radial stress

$$\sigma_{rr}^0(a,z) < 0, \quad z_2 \leqslant |z| < \infty, \tag{2j}$$

and the absolute value of the shear stress is such that it does not allow slip.

The boundary conditions at the matrix edge $r = c$ are given by

$$u_r^1(c,z) = u_r^{1T}(c,z) + u_r^{1\varepsilon}(c,z), \quad 0 \leqslant |z| < \infty, \tag{3}$$

$$\sigma_{rz}^1(c,z) = 0, \quad 0 \leqslant |z| \infty, \tag{4}$$

where u_r^{1T} is the radial displacement in the uncracked composite due to a temperature change, ΔT and $u_r^{1\varepsilon}$ is the radial displacement in the uncracked composite due to a remote axial strain, ε_0 (see Appendices A and B).

The boundary condition, eqn (3), results in the slope of the crack surface $\partial u_z^1(r,0)/\partial r|_{r=e}$ equal to zero for the edge crack problem ($e = c$). Moreover, at the edge $r = c$, far away from the crack plane, this boundary condition, eqn (3), gives zero radial stresses.

The shear stress in the composite cylinder at the crack plane $z = 0$ is

$$\sigma_{rz}^0(r,0) = 0, \quad r \leqslant a, \tag{5a}$$

$$\sigma_{rz}^1(r,0) = 0, \quad a \leqslant r \leqslant c. \tag{5b}$$

The other boundary conditions at the crack plane $z = 0$ are

$$u_z^0(r,0) = 0, \quad r \leqslant a, \tag{6a}$$

$$u_z^1(r,0) = 0, \quad a \leqslant r < d, \quad e < r \leqslant c, \tag{6b}$$

$$\sigma_{zz}^1(r,0) = 0, \quad d < r < e, \tag{6c}$$

constrained by the opening of the transverse crack

$$u_z^1(r,0) > 0, \quad d < r < e. \tag{7}$$

Formulation

The solution for the above problem is obtained by a related boundary element method. The composite cylinder geometry of Fig. 1 can be viewed as two auxiliary bodies, as shown in Fig. 2.

The first diagram is that of a solid cylinder with unknown surface tractions on the boundary $r = a$. The second diagram is that of a hollow cylinder with unknown surface tractions on the inner radius $r = b$ ($b = a$ in the composite cylinder) an unknown slope of the crack-opening displacement at $z = 0$, and known boundary conditions on the outer radius $r = c$.

The complete displacement and stress fields of the solid cylinder (fiber) can be now found in terms of the unknown surface tractions at $r = a$. For the hollow cylinder (matrix), the complete displacement and stress fields can also be found in terms of the unknown tractions at $r = b$ and the unknown slope of the crack-opening displacement at $z = 0$. Once these field equations are obtained, the continuity and boundary conditions, eqns (1)–(7), can be applied to find the solution in terms of coupled integral equations. These coupled

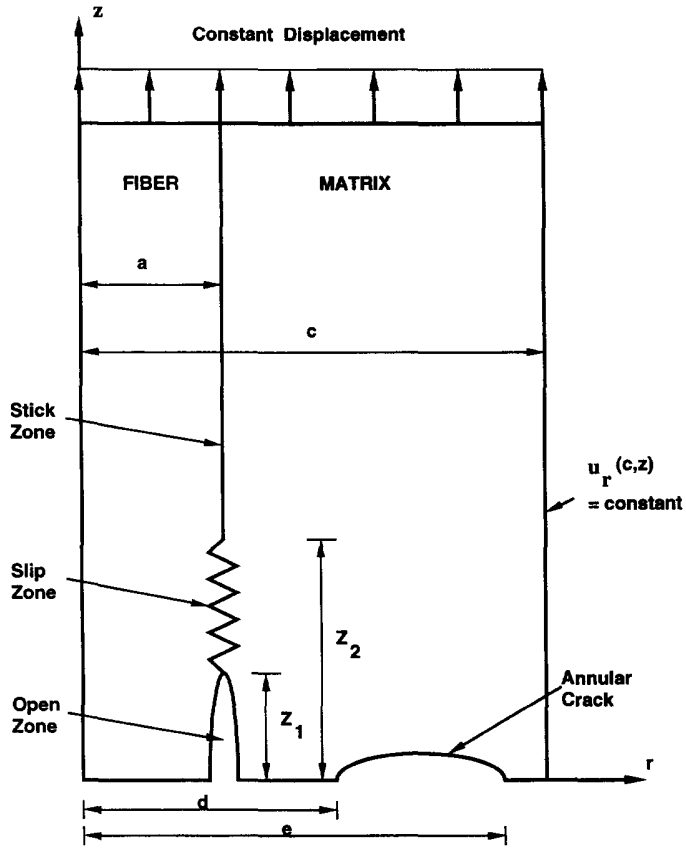

Fig. 1. Schematic of a representative volume element of a brittle matrix composite with a frictional interface and annular matrix crack under a thermomechanical load.

equations can then be solved numerically to find the stress/displacement field in the entire composite geometry.

Field equations for the solid cylinder. The displacement/stress field for an axisymmetric solid cylinder of radius a, shear modulus μ_0, and Poisson's ratio ν_0 and which has symmetry about the $z = 0$ plane with boundary stresses

$$\sigma^0_{rr}(a, z) = S_0(z), \quad 0 < z < \infty, \tag{8a}$$

$$\sigma^0_{rz}(a, z) = T_0(z), \quad 0 < z < \infty, \tag{8b}$$

where $S_0(z)$ and $T_0(z)$ are absolutely integrable in $(0, \infty)$, is given by:

$$\begin{aligned} M^0_i(r, z) = {} & \frac{2}{\pi}\int_0^\infty [k_{1i}(r, s) - k^\infty_{1i}(r, s)]\,\mathrm{cossin}\,(zs)\,\mathrm{d}s \int_0^\infty T_0(t)\sin(st)\,\mathrm{d}t \\ & + \frac{2}{\pi}\int_0^\infty T_0(t)\,\mathrm{d}t \int_0^\infty k^\infty_{1i}(r, s)\,\mathrm{cossin}\,(zs)\sin(st)\,\mathrm{d}s \\ & + \frac{2}{\pi}\int_0^\infty [k_{2i}(r, s) - k^\infty_{2i}(r, s)]\,\mathrm{cossin}\,(zs)\,\mathrm{d}s \int_0^\infty S_0(t)\cos(st)\,\mathrm{d}t \\ & + \frac{2}{\pi}\int_0^\infty S_0(t)\,\mathrm{d}t \int_0^\infty k^\infty_{2i}(r, s)\,\mathrm{cossin}\,(zs)\cos(st)\,\mathrm{d}s, \quad i = 1, \ldots, 6, \end{aligned} \tag{9}$$

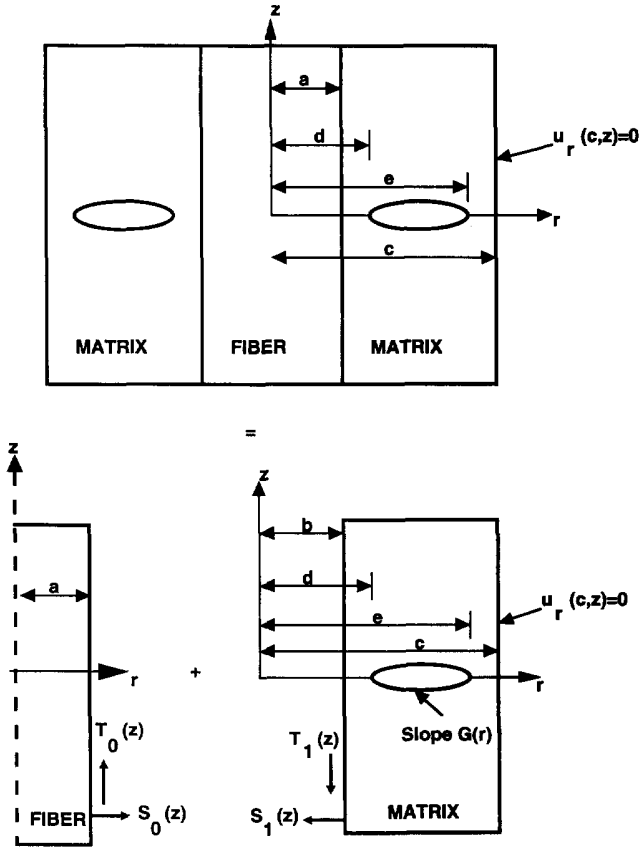

Fig. 2. Schematic diagrams of fiber and matrix with unknown surface tractions and slope of crack-opening displacement.

where M_1 = radial displacement, $u_r(r, z)$,
M_2 = axial displacement, $u_z(r, z)$,
M_3 = radial stress, $\sigma_{rr}(r, z)$,
M_4 = axial stress, $\sigma_{zz}(r, z)$,
M_5 = shear stress, $\sigma_{rz}(r, z)$,
M_6 = hoop stress, $\sigma_{\theta\theta}(r, z)$,
cossin (zs) = cos (zs), if $i = 1, 3, 4, 6$,
= sin (zs), if $i = 2, 5$,
and $k_{1i}, k_{1i}^{\infty}, k_{2i}, k_{2i}^{\infty}$ are as given in Appendix C.

Field equations for the hollow cylinder. The displacement/stress field for an axisymmetric hollow cylinder of inner radius b, outer radius c, shear modulus μ_1, and Poisson's ratio ν_1, symmetric about the $z = 0$ plane with boundary conditions

$$\sigma_{rr}^1(b, z) = S_1(z), \quad 0 \leqslant z < \infty, \tag{10a}$$

$$\sigma_{rz}^1(b, z) = T_1(z), \quad 0 \leqslant z < \infty, \tag{10b}$$

$$u_r^1(c, z) = 0, \quad 0 \leqslant z < \infty, \tag{10c}$$

$$\sigma_{rz}^1(c, z) = 0, \quad 0 \leqslant z < \infty, \tag{10d}$$

$$\frac{\mu_1}{1-\nu_1}\frac{\partial}{\partial r}u_z^1(r, 0) = \phi(r), \quad d < r < e, \tag{10e}$$

$$u_z^1(r, 0) = 0, \quad b < r < d, \quad e < r < c, \tag{10f}$$

where $S_1(z)$ and $T_1(z)$ are absolutely integrable in $(0, \infty)$ and $\phi(r)$ is integrable in (d, e), is given by

$$
\begin{aligned}
M_i^1(r,z) = & \int_0^\infty [p_{1i}(r,s) - p_{1i}^\infty(r,s)] \operatorname{cossin}(zs)\,\mathrm{d}s \int_0^\infty T_1(t)\sin(st)\,\mathrm{d}t \\
& + \int_0^\infty T_1(t)\,\mathrm{d}t \int_0^\infty p_{1i}^\infty(r,s)\operatorname{cossin}(zs)\sin(st)\,\mathrm{d}s \\
& + \int_0^\infty S_1(t)\,\mathrm{d}t \int_0^\infty p_{2i}^\infty(r,s)\operatorname{cossin}(zs)\cos(st)\,\mathrm{d}s \\
& + \int_0^\infty [p_{2i}(r,s) - p_{2i}^\infty(r,s)] \operatorname{cossin}(zs)\,\mathrm{d}s \int_0^\infty S_1(t)\cos(st)\,\mathrm{d}t \\
& + \int_d^e \phi(t)\,\mathrm{d}t \int_0^\infty [p_{3i}(r,s,t) - p_{3i}^{b\infty}(r,s,t) - p_{3i}^{c\infty}(r,s,t)] \operatorname{cossin}(zs)\,\mathrm{d}s \\
& + \int_d^e \phi(t)\,\mathrm{d}t \int_0^\infty \{[p_{3i}^{b\infty}(r,s,t) + p_{3i}^{c\infty}(r,s,t)] \operatorname{cossin}(zs)\,\mathrm{d}s \\
& + N_i(r,t,z)\}, \quad i = 1,\ldots,6,
\end{aligned} \tag{11}
$$

where $p_{1i}, p_{1i}^\infty, p_{2i}, p_{2i}^\infty, p_{3i}, p_{3i}^\infty$ and N_i are as given in Appendix C.

The above stress and displacement field equations (9) and (11) for the solid and hollow cylinder are restricted by the condition of absolute integrability of the tractions. These field equations cannot therefore directly represent non-vanishing stresses and strains due to temperature change and remote uniform strain as $z \to \infty$. However, the stresses as $z \to \infty$ are independent of the matrix crack and interfacial friction (provided that z_2 is finite). These stresses and displacements are those due to the temperature change and remote strain in the undamaged composite cylinder. Hence the complete stress and displacement field of the solid and the hollow cylinder in the presence of a temperature change and remote uniform strain in the composite cylinder are given by:

$$u_r^j(r,z) = M_1^j(r,z) + u_r^{jT}(r,z) + u_r^{j\varepsilon}(r,z), \quad j = 0,1, \tag{12a}$$

$$u_z^j(r,z) = M_2^j(r,z) + u_z^{jT}(r,z) + u_z^{j\varepsilon}(r,z), \quad j = 0,1, \tag{12b}$$

$$\sigma_{rr}^j(r,z) = M_3^j(r,z) + \sigma_{rr}^{jT}(r,z) + \sigma_{rr}^{j\varepsilon}(r,z), \quad j = 0,1, \tag{12c}$$

$$\sigma_{zz}^j(r,z) = M_4^j(r,z) + \sigma_{zz}^{jT}(r,z) + \sigma_{zz}^{j\varepsilon}(r,z), \quad j = 0,1, \tag{12d}$$

$$\sigma_{rz}^j(r,z) = M_5^j(r,z), \quad j = 0,1, \tag{12e}$$

$$\sigma_{\theta\theta}^j(r,z) = M_6^j(r,z) + \sigma_{\theta\theta}^{jT}(r,z) + \sigma_{\theta\theta}^{j\varepsilon}(r,z), \quad j = 0,1. \tag{12f}$$

In the above equations (12), the second and third terms on the right-hand side are the known stresses and displacements due to the temperature change, ΔT, and axial remote strain, ε_0, respectively, in the undamaged composite cylinder and are given in Appendices A and B. The superscript T corresponds to the effect of temperature change, ΔT; the superscript ε corresponds to the effect of the axial remote tensile strain, ε_0.

Now, the interface and boundary conditions, eqns (1)–(7), can be applied to give integral equations with S_0, T_0, S_1, T_1, and ϕ as the five unknown functions. These equations can be solved simultaneously to find the five unknown functions. The numerical scheme to find these functions is given in the next section.

NUMERICAL SCHEME

The numerical scheme is discussed first for the case of an annular edge crack not touching the interface ($d > a$, $e = c$). The changes required for the numerical scheme for other cases follow at the end of this section.

Internal edge crack ($d > a$, $e = c$)

The application of the boundary and continuity conditions as given by eqns (1)–(7) should give the values of the interface stresses, T_0, S_0, T_1, and S_1 and the slope of the crack-opening displacement function, ϕ. This is done as follows.

Assume that the range of $0 < z < \infty$ is divided into n unequal segments

$$T_0(z) = A_i + B_i z, \quad \omega_i < z < \omega_{i+1}, \quad i = 1, 2 \ldots n-1, \tag{13a}$$

$$= B_n/z^3, \quad \omega_n < z < \infty,$$

$$S_0(z) = C_i + D_i z, \quad \omega_i < z < \omega_{i+1}, \quad i = 1, 2 \ldots n-1, \tag{13b}$$

$$= D_n/z^3, \quad \omega_n < z < \infty,$$

$$T_1(z) = P_i + Q_i z, \quad \omega_i < z < \omega_{i+1}, \quad i = 1, 2 \ldots n-1, \tag{13c}$$

$$= Q_n/z^3, \quad \omega_n < z < \infty,$$

$$S_1(z) = R_i + S_i z, \quad \omega_i < z < \omega_{i+1}, \quad i = 1, 2 \ldots n-1, \tag{13d}$$

$$= S_n/z^3, \quad \omega_n < z < \infty.$$

The $1/z^3$ behavior is assumed in the above stress expressions, eqns (13), in the last segment because it simulates the behavior of a stress field as z becomes large (Schweitert and Steif, 1991).

Further assume that the range (d, e) of the crack is divided into m unequal segments such that $r_1 = d$ and $r_{m+1} = e$, and

$$\phi(r) = (U_i + V_i r) w(r), \quad r_i < r < r_{i+1}, \quad i = 1, 2 \ldots, m, \tag{14a}$$

where

$$w(r) = \frac{1}{\sqrt{r-d}}, \tag{14b}$$

is the weight function denoting the singularity of the slope of the crack-opening displacement at the crack tip ($r = d$). The problem hence reduces to finding the values of the constants A_i, B_i, C_i, D_i, P_i, Q_i, R_i, S_i, U_i, and V_i in eqns (13) and (14).

On substituting the expressions for the tractions and slope given by eqns (13) and (14) in eqns (9) and (11), the radial and axial displacements at the interface ($r = a$) in the two bodies 0 and 1, and the axial stress in body 1 on the $z = 0$ plane can be written as

$$u_r^0(a, z) = \sum_{i=1}^{n-1} A_i X_{i1}(z) + \sum_{i=1}^{n} B_i X_{i2}(z) + \sum_{i=1}^{n-1} C_i X_{i3}(z) + \sum_{i=1}^{n} D_i X_{i4}(z), \tag{15a}$$

$$u_z^0(a, z) = \sum_{i=1}^{n-1} A_i X_{i5}(z) + \sum_{i=1}^{n} B_i X_{i6}(z) + \sum_{i=1}^{n-1} C_i X_{i7}(z) + \sum_{i=1}^{n} D_i X_{i8}(z), \tag{15b}$$

$$u_r^1(b, z) = \sum_{i=1}^{n-1} P_i Y_{i1}(z) + \sum_{i=1}^{n} Q_i Y_{i2}(z) + \sum_{i=1}^{n-1} R_i Y_{i3}(z) + \sum_{i=1}^{n} S_i Y_{i4}(z)$$

$$+ \sum_{i=1}^{m} U_i Y_{i5}(z) + \sum_{i=1}^{m} V_i Y_{i6}(z), \tag{15c}$$

$$u_z^1(b,z) = \sum_{i=1}^{n-1} P_i Y_{i7}(z) + \sum_{i=1}^{n} Q_i Y_{i8}(z) + \sum_{i=1}^{n-1} R_i Y_{i9}(z) + \sum_{i=1}^{n} S_i Y_{i10}(z) + \sum_{i=1}^{m} U_i Y_{i11}(z) + \sum_{i=1}^{m} V_i Y_{i12}(z), \quad (15d)$$

$$\sigma_{zz}^1(r,0) = \sum_{i=1}^{n-1} P_i Z_{i1}(r) + \sum_{i=1}^{n} Q_i Z_{i2}(r) + \sum_{i=1}^{n-1} R_i Z_{i3}(r) + \sum_{i=1}^{n} S_i Z_{i4}(r) + \sum_{i=1}^{m} U_i Z_{i5}(r) + \sum_{i=1}^{m} V_i Z_{i6}(r), \quad (15e)$$

where X_{ij} and Y_{ij} are functions of z, and Z_{ij} is a function of r.

The interface zone ($0 < z < \infty$) and the crack zone ($d < r < e$) are divided into n and m segments, respectively. The segment points along the interface zone are chosen as

$$\begin{aligned}
\omega_i &= -\cos\left(\frac{i-1}{n_o}\pi\right)\frac{z_1}{2} + \frac{z_1}{2}, && i = 1,\ldots,n_o,\\
&= -\cos\left(\frac{i-n_o-1}{n_s}\pi\right)\frac{(z_2-z_1)}{2} + \frac{(z_2+z_1)}{2}, && i = n_o+1,\ldots,n_o+n_s,\\
&= -\cos\left(\frac{i-n_o-n_s-1}{n_t-1}\frac{\pi}{2}\right)(z_3-z_2)+z_3, && i = n_o+n_s+1,\ldots,n,
\end{aligned} \quad (16a)$$

where z_1 = length of the open zone,
$z_2 - z_1$ = length of the slip zone,
z_3 = maximum $[n^* z_2, n^*(c-b)+z_2]$,
n^* = a number chosen large enough for the stress field to be (nearly) independent of z for $z > z_3$. Note that $z_3 = \omega_n$.

The segment points along the crack surface are chosen as

$$\psi_i = \frac{e-d}{2}x_i + \frac{e+d}{2}, \quad i = 1,\ldots,m, \quad (16b)$$

where x_i = the ith root of the mth order Legendre polynomial equal to zero.

The above choice of segment points in eqns (16) allows a concentration of segments near the transition points, such as at the end of the open and slip zones, and at the transverse crack tip. The segments n_o, n_s, and n_t are the number of segments in the open, slip, and stick zones of the interface, respectively. Hence the total number of segments at the interface ($r = a$) is

$$n = n_o + n_s + n_t. \quad (17)$$

The collocation points along the interface (except the last one) and along the transverse crack are chosen at the midpoint of the segments as

$$\Omega_i = (\omega_i + \omega_{i+1})/2, \quad i = 1,\ldots,n-1,$$
$$\Omega_n = \omega_{n-1} + 2(\omega_n - \omega_{n-1}), \quad (18a)$$
$$\zeta_i = (\psi_i + \psi_{i+1})/2, \quad i = 1,\ldots,m. \quad (18b)$$

There are $(8n-4+2m)$ unknowns, and one needs to set up the same number of equations. These are generated as follows.

1. The interface shear stresses T_0 and T_1, the interface normal stresses S_0 and S_1, and the crack slope function $\phi(r)$ are assumed to be continuous at all points. These points include the segment points that give $(2n+m-3)$ equations.
Continuity of shear tractions along the interface at segment points ω_i gives

$$A_i + B_i\omega_{i+1} = A_{i+1} + B_{i+1}\omega_{i+1}, \quad i = 1, \ldots, n-2, \tag{19a}$$

$$A_{n-1} + B_{n-1}\omega_n = B_n/\omega_n^3. \tag{19b}$$

Continuity of normal tractions along the interface at segment points ω_i gives

$$C_i + D_i\omega_{i+1} = C_{i+1} + D_{i+1}\omega_{i+1}, \quad i = 1, \ldots, n-2, \tag{19c}$$

$$C_{n-1} + D_{n-1}\omega_n = D_n/\omega_n^3. \tag{19d}$$

Continuity of slope functions $\phi(r)$ along the transverse crack at segment points ψ_i gives

$$U_i + V_i\psi_{i+1} = U_{i+1} + V_{i+1}\psi_{i+1}, \quad i = 1, \ldots, m-1. \tag{19e}$$

Note that there are no singularities in the interface stresses if the interface follows the Coulomb friction law.

2. The continuity conditions (1) of shear and normal tractions at $r = a$ give $(4n-2)$ equations:

$$A_i = P_i, \quad C_i = R_i, \quad i = 1, \ldots, n-1, \tag{20a}$$

$$B_i = Q_i, \quad D_i = S_i, \quad i = 1, \ldots, n. \tag{20b}$$

3. The open zone condition, eqn (2a), of zero shear stress gives (n_o) equations as

$$A_i + B_i\Omega_i = 0, \quad i = 1, \ldots, n_o. \tag{21}$$

4. The open zone condition, eqn (2b), of zero normal tractions gives (n_o) equations as

$$C_i + D_i\Omega_i = -[\sigma_{rr}^{0T}(a, \Omega_i) + \sigma_{rr}^{0\varepsilon}(a, \Omega_i)], \quad i = 1, \ldots, n_o. \tag{22}$$

5. The Coulomb friction law in the slip zone condition, eqn (2e), gives (n_s) equations as

$$A_i + B_i\Omega_i + \rho(C_i + D_i\Omega_i) = -\rho[\sigma_{rr}^{0T}(a, \Omega_i) + \sigma_{rr}^{0\varepsilon}(a, \Omega_i)], \quad i = n_o+1, \ldots, n_o+n_s. \tag{23}$$

6. The radial displacement continuity conditions, eqns (2d) and (2h), in the slip and stick zone gives (n_s+n_t) equations from eqns (15a) and (15c), as

$$\sum_{i=1}^{n-1} A_i X_{i1}(\Omega_j) + \sum_{i=1}^{n} B_i X_{i2}(\Omega_j) + \sum_{i=1}^{n-1} C_i X_{i3}(\Omega_j) + \sum_{i=1}^{n} D_i X_{i4}(\Omega_j)$$
$$- \sum_{i=1}^{n-1} P_i Y_{i1}(\Omega_j) - \sum_{i=1}^{n} Q_i Y_{i2}(\Omega_j) - \sum_{i=1}^{n-1} R_i Y_{i3}(\Omega_j) - \sum_{i=1}^{n} S_i Y_{i4}(\Omega_j)$$
$$- \sum_{i=1}^{m} U_i Y_{i5}(\Omega_j) - \sum_{i=1}^{m} V_i Y_{i6}(\Omega_j) = 0, \quad j = n_o+1, \ldots, n. \tag{24}$$

7. The axial displacement continuity condition, eqn (2i), in the stick zone gives (n_t) equations from eqns (15b) and (15d) as

$$\sum_{i=1}^{n-1} A_i X_{i5}(\Omega_j) + \sum_{i=1}^{n} B_i X_{i6}(\Omega_j) + \sum_{i=1}^{n-1} C_i X_{i7}(\Omega_j) + \sum_{i=1}^{n} D_i X_{i8}(\Omega)_j$$

$$- \sum_{i=1}^{n-1} P_i Y_{i7}(\Omega_j) - \sum_{i=1}^{n} Q_i Y_{i8}(\Omega_j) - \sum_{i=1}^{n-1} R_i Y_{i9}(\Omega_j) - \sum_{i=1}^{n} S_i Y_{i10}(\Omega_j)$$

$$- \sum_{i=1}^{m} U_i Y_{i11}(\Omega_j) - \sum_{i=1}^{m} V_i Y_{i12}(\Omega_j) = 0, \quad j = n_o + n_s + 1, \ldots, n. \tag{25}$$

8. The traction-free crack surface condition, eqn (7), gives (m) equations from eqn (15e) as

$$\sum_{i=1}^{n-1} P_i Z_{i1}(\zeta_j) + \sum_{i=1}^{n} Q_i Z_{i2}(\zeta_j) + \sum_{i=1}^{n-1} R_i Z_{i3}(\zeta_j) + \sum_{i=1}^{n} S_i Z_{i4}(\zeta_j)$$

$$+ \sum_{i=1}^{m} U_i Z_{i5}(\zeta_j) + \sum_{i=1}^{m-1} V_i Z_{i6}(\zeta_j) = -[\sigma_{zz}^{1T}(\zeta_j, 0) + \sigma_{zz}^{1p}(\zeta_j, 0)], \quad j = 1, \ldots, m. \tag{26}$$

9. Since $u_r(c, z)$ is a constant as given by eqn (3), the slope of the crack-opening displacement $(\partial/\partial r)u_z(r, 0)$ at the outer edge ($r = e$) of the hollow cylinder is zero. From eqns (10e) and (14a), we have

$$U_m + cV_m = 0. \tag{27}$$

The total number of equations (19)–(27) is $(8n-4+2m)$. These are solved simultaneously to calculate the unknown functions. One can then substitute these values in eqn (12) to find the displacements and stresses at any point in the composite cylinder.

The stress intensity factor (SIF) of the crack tip ($r = d$) is given by

$$K = \lim_{r \to d-} \sqrt{2(d-r)}\,\sigma_{zz}^{1}(r, 0). \tag{28a}$$

According to Gupta (1973), the SIF can be written as

$$K = \frac{\mu_1}{2(1-\nu_1)} \lim_{r \to d+} \sqrt{2(r-d)}\,\frac{\partial}{\partial r} u_z^{1}(r, 0) = \frac{1}{\sqrt{2}}(U_1 + V_1 d). \tag{28b}$$

The crack-opening displacement $u_z(r, 0+)$, $d < r < c$, at any point along the crack is given by integrating the slope function as defined by equation (10e):

$$u_z(r, 0+) = \frac{1-\nu_1}{\mu_1} \int_d^r \phi(r)\,\mathrm{d}r$$

$$= \frac{1-\nu_1}{\mu_1} \sum_{i=1}^{m} U_i \int_{r_i}^{r_{i+1}} w(r)\,\mathrm{d}r + \sum_{i=1}^{m} V_i \int_{r_i}^{r_{i+1}} r w(r)\,\mathrm{d}r. \tag{28c}$$

Edge crack touching the slipping or open interface ($d = a$, $e = c$)

This case is different from the previous one, since the edge crack is now touching an interface that is slipping or open. The singularity at the crack tip vanishes in the slope function $\phi(r)$ (Dundurs and Comninou, 1979). Furthermore, since the hollow cylinder now has a through crack, one needs both to establish equilibrium of forces and prevent any rigid body displacements of the hollow cylinder. The following steps are taken differently from eqns (13)–(27) to account for the above differences.

1. Since the crack goes through the axial plane $z = 0$, the force equilibrium is enforced in the axial direction in the hollow matrix cylinder. This is given by

$$-\int_0^\infty \sigma_{rz}^1(a,z)2\pi b\,\mathrm{d}z+[\sigma_{zz}^{1T}(r,\infty)+\sigma_{zz}^{1\varepsilon}(r,\infty)]\pi(c^2-b^2)=0. \tag{29a}$$

Substituting eqn (13c) into eqn (29a), we obtain

$$\sum_{j=1}^{n-1} 2\pi b(\omega_{j+1}-\omega_j)P_j+\sum_{j=1}^{n-1}\pi b(\omega_{j+1}^2-\omega_j^2)Q_j+\frac{1}{2\omega_n^2}Q_n = [\sigma_{zz}^{1T}(r,\infty)+\sigma_{zz}^{1\varepsilon}(r,\infty)]\pi(c^2-b^2). \tag{29b}$$

The nth equation of eqn (25) is replaced by eqn (29b). Note that, in the cases studied here, $a = b$.

2. The weight function of eqn (14b) is $w(r) = 1$, since the shear stress is antisymmetric and zero at ($r = b$, $z = 0$). The absence of any singularities for relevant values of the elastic moduli and friction coefficient, ρ, for ceramic matrix composites is discussed by Schweitert and Steif (1991). If the interface is open at $z = 0$, singularities again do not exist in the slope function $\phi(r)$ (Lu and Erdogan, 1984).
3. Since the hollow cylinder has a through crack, it can have a rigid body displacement in the z direction. The first $(n-n_0-n_s-1)$ equations of eqn (25) are hence replaced by the continuity of the axial displacement differences at the interface as

$$u_z^0(a,\Omega_j)-u_z^0(a,\Omega_{j+1}) = u_z^1(a,\Omega_j)-u_z^1(a,\Omega_{j+1}),\quad j = n_o+n_s+1,\ldots,n-1,$$

which gives

$$\begin{aligned}
&\sum_{i=1}^{n-1} A_iX_{i5}(\Omega_j)+\sum_{i=1}^{n} B_iX_{i6}(\Omega_j)+\sum_{i=1}^{n-1} C_iX_{i7}(\Omega_j)+\sum_{i=1}^{n} D_iX_{i8}(\Omega_j)\\
&\quad-\sum_{i=1}^{n-1} A_iX_{i5}(\Omega_{j+1})-\sum_{i=1}^{n} B_iX_{i6}(\Omega_{j+1})-\sum_{i=1}^{n-1} C_iX_{i7}(\Omega_{j+1})-\sum_{i=1}^{n} D_iX_{i8}(\Omega_{j+1})\\
&\quad-\sum_{i=1}^{n-1} P_iY_{i7}(\Omega_j)-\sum_{i=1}^{n} Q_iY_{i8}(\Omega_j)-\sum_{i=1}^{n-1} R_iY_{i9}(\Omega_j)-\sum_{i=1}^{n} S_iY_{i10}(\Omega_j)\\
&\quad-\sum_{i=1}^{m} U_iY_{i11}(\Omega_j)-\sum_{i=1}^{m} V_iY_{i12}(\Omega_j)\\
&\quad+\sum_{i=1}^{n-1} P_iY_{i7}(\Omega_{j+1})+\sum_{i=1}^{n} Q_iY_{i8}(\Omega_{j+1})+\sum_{i=1}^{n-1} R_iY_{i9}(\Omega_{j+1})+\sum_{i=1}^{n} S_iY_{i10}(\Omega_{j+1})\\
&\quad+\sum_{i=1}^{m} U_iY_{i11}(\Omega_{j+1})+\sum_{i=1}^{m} V_iY_{i12}(\Omega_{j+1}) = 0,\quad j = n_o+n_s+1,\ldots,n-1.
\end{aligned} \tag{30}$$

4. The shear stress at $z = z_1$ is exactly zero and is enforced by replacing the nth equation of eqn (24) as $\tau_{rz}(b,z_1) = 0$:

$$P_{n_o+1}+Q_{n_o+1}\omega_{n_o+1} = -\rho[\sigma_{rr}^{1T}(a,\omega_{n_o+1})+\sigma_{rr}^{1\varepsilon}(a,\omega_{n_o+1})]. \tag{31}$$

Again, for the above case, there are $(8n-4+2m)$ equations and an equal number of unknowns.

The input remote strain ε_0 is required to satisfy all the inequality and sign conditions of eqns (2c), (2f), (2g), (2k) and (7). In the procedure established, the strain ε_0 is changed

iteratively until it satisfies all the inequality conditions for constant values of the length of the open and slip zones. It is quite possible that a small range of strain ε_0 may satisfy all the equations, including the inequality conditions. The correct ε_0 is selected by the unique value, where the shear stress at the open–slip ($z = z_1$) and slip–stick transitions ($z = z_2$) is smooth, that is:

$$\frac{\mathrm{d}}{\mathrm{d}z}\tau_{rz}^1(a,z)|_{z_2-} = \frac{\mathrm{d}}{\mathrm{d}z}\tau_{rz}^1(a,z)|_{z_2+},$$

or

$$Q_{n_0+n_s} = Q_{n_0+n_s+1}. \tag{32a}$$

and

$$\frac{\mathrm{d}}{\mathrm{d}z}\tau_{rz}^1(a,z)|_{z_1-} = \frac{\mathrm{d}}{\mathrm{d}z}\tau_{rz}^1(a,z)|_{z_1+},$$

or

$$Q_{n_0} = Q_{n_0+1}. \tag{33}$$

This smoothness of the shear stress at the slip–stick transition is implied by the asymptotic analysis of Dundurs and Comninou (1979) at the slip–stick transition in a frictional interface between two dissimilar elastic half-planes.

The crack-opening displacement $u_z^1(r,0+)$, $d < r < c$, at any point along the crack is given by integrating the slope function as defined by eqn (10*e*):

$$u_z^1(r,0+) - u_z^1(a,0+) = \frac{1-\nu_1}{\mu_1}\int_d^r \phi(r)\,\mathrm{d}r$$

$$= \frac{1-\nu_1}{\mu_1}\sum_{i=1}^{m} U_i[r_{i+1}-r_i] + \sum_{i=1}^{m}\frac{V_i}{2}[r_{i+1}^2 - r_i^2]. \tag{34}$$

Note that $u_z^1(a,0+)$ can be calculated by using eqn (12), but it includes a rigid-body displacement term. This constant rigid-body term can be found by knowing that

$$u_z^0(a,z_2+) - u_z^1(a,z_2+) = 0, \tag{35a}$$

as per eqn (2i) and

$$u_z^0(r,0) = 0, \quad 0 < r < a, \tag{35b}$$

as per eqn (6a).

Closed crack in the matrix ($d > a, e < c$)

This case is again different from the internal edge case. The main difference is that the crack is closed, and one needs to satisfy the crack closure condition for uniqueness of the solution. The following steps are different for this case from those given by eqns (13)–(27).

Equation (27) is replaced by the closed crack condition

$$\int_d^e \phi(r)\,\mathrm{d}r = 0, \tag{36a}$$

which gives

$$\sum_{i=1}^{m} U_i \int_{r_i}^{r_{i+1}} w(r)\,\mathrm{d}r + \sum_{i=1}^{m} V_i \int_{r_i}^{r_{i+1}} rw(r)\,\mathrm{d}r = 0, \quad i = 1, \ldots, m, \tag{36b}$$

where

$$w(r) = \frac{1}{\sqrt{(r-d)(e-r)}}. \tag{36c}$$

For this case, there are $(8n-4+2m)$ unknowns and an equal number of equations. Hence the system of simultaneous linear equations can be solved.

The crack-opening displacement $u_z(r, 0+)$, $d < r < e$, at any point along the crack is given by eqn (28c).

The stress intensity factors at the two crack tips ($r = d$) and ($r = e$) are found similarly to eqn (28) as

$$K(r = d) = \lim_{r \to d-} \sqrt{2(d-r)}\sigma_{zz}^{1}(r, 0) = \frac{1}{\sqrt{2}} \frac{(U_1 + V_1 d)}{\sqrt{e-d}}, \tag{37a}$$

and

$$K(r = e) = \lim_{r \to e+} \sqrt{2(r-e)}\,\sigma_{zz}^{1}(r, 0) = -\frac{1}{\sqrt{2}} \frac{(U_m + V_m e)}{\sqrt{e-d}}. \tag{37b}$$

For each of the above three cases, the solution can be substituted in eqn (12) to obtain the stress and displacement field in the fiber and the matrix.

The computer program for this study is computationally very intensive. For typical values of 48 segments on the interface zone and 11 on the transverse crack surface, it takes about 15 hours of CPU time on an IBM 3090 computer for calculation of the slip lengths, and an extra 15 hours of CPU time for calculation of the critical stresses/displacements in the composite geometry. Hence limited results are presented in this paper.

We have, however, taken advantage of the method described in this paper to return to some of the intermediate results to solve the problem for different values of the remote strain, ε_0, temperature change, ΔT, friction coefficient, ρ, and coefficients of thermal expansion, α_0 and α_1. This is done as follows. The most computationally intensive part of the computer program is calculation of the elements of eqn (15) at the collocation points. However, once the $(8n-4+2m)$ equations are set up, the remote strain, ε_0, the temperature change, ΔT, the friction coefficient, ρ, and the coefficients of thermal expansion, α_0 and α_1, can be changed in these equations. These parameters do not change the coefficient matrix elements corresponding to eqn (15). Other elements of the coefficient matrix and the right-hand sides, which do need to be changed, require only a few seconds of computational time.

RESULTS AND DISCUSSION

The numerical scheme presented in this study was tested as follows. Extensive convergence studies were made to find the number of collocation points to be used. In addition to numerical tests such as recovering applied stresses on the two bodies, comparisons with some exact models were also made. These tests included comparing the stress intensity factor for a small edge crack under uniform pressure, p, which is $p\sqrt{2(e-d)}$ (Sneddon, 1951). For edge cracks comparable with the thickness, $(c-b)$, of the hollow cylinder inside the matrix, the results for the stresses and the stress intensity factors compared well with Figs 11–14 of the paper by Wijeyewickrema and Keer (1991). For an actual numerical comparison, an independent computer program was written for the problem solved by Wijeyewickrema and Keer (1991) by using numerical methods reported by Kaw and Pagano

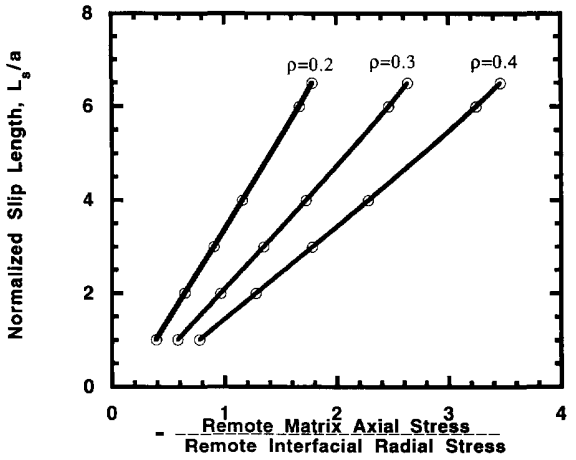

Fig. 3. Normalized slip length as a function of the negative of the ratio of the remote matrix axial stress to the remote interfacial radial stress for constant coefficients of friction.

(1993). The results of the present model agreed within $\pm 5\%$ of the numerical results of Wijeyewickrema and Keer (1991).

The SiC (silicon carbide)/CAS (calcium aluminosilicate glass ceramic) material system with the following elastic properties is used to discuss the results. These values were taken from the experimental work of Daniel *et al.* (1989).

Silicon carbide fiber:
$E_0 = 207\,\text{GPa}$
$\nu_0 = 0.25.$

Calcium aluminosilicate glass matrix:
$E_1 = 98\,\text{GPa}$
$\nu_1 = 0.25$
$V_f = 0.4.$

Only cases with slip and no open zone, and $d = a$, $e = c$, are considered in this study. This is because, for cases in which both types of zone are possible, there are two variables, the length of the open zone and the length of the slip zone, which need to be found iteratively. Finding these two variables is computationally possible with the current computer program but would require a prohibitive amount of computational time. Furthermore, the Poisson's ratios are equal in the fiber and the matrix in the SiC/CAS material system, but the present model does allow unequal Poisson's ratios of the fiber and the matrix.

Figure 3 shows the normalized slip length, L_s/a as a function of the ratio of the negative value of the matrix axial stress to the interfacial radial stress (ARS),

$$\text{ARS} = -[\sigma_{zz}^{1T}(r, \infty) + \sigma_{zz}^{1\varepsilon}(r, \infty)]/[\sigma_{rr}^{1T}(a, \infty) + \sigma_{rr}^{1\varepsilon}(a, \infty)], \tag{38}$$

for a constant coefficient of friction. The reason for choosing the abscissa as the ratio of the stresses ARS is because any combination of temperature change, remote axial strain, and linear coefficients of thermal expansion of the fiber and the matrix that result in the same stress ratio (ARS) will result in the same slip length. Also note that the remote axial strain, ε_0, is the applied mechanical strain, and there is a separate contribution to the normal strain in the z-direction that is due the temperature change, ΔT.

In Fig. 3, the slip length increases monotonically with an increase in stress ratio, ARS, and decreases monotonically with an increase in coefficient of friction. Note that the slip length was also found (not shown) to be a monotonically increasing function of the remote axial strain since the stress $\sigma_{rr}^{1\varepsilon}(a, z) = 0$ for equal values of the Poisson's ratio of the fiber and the matrix in the SiC/CAS material system used here.

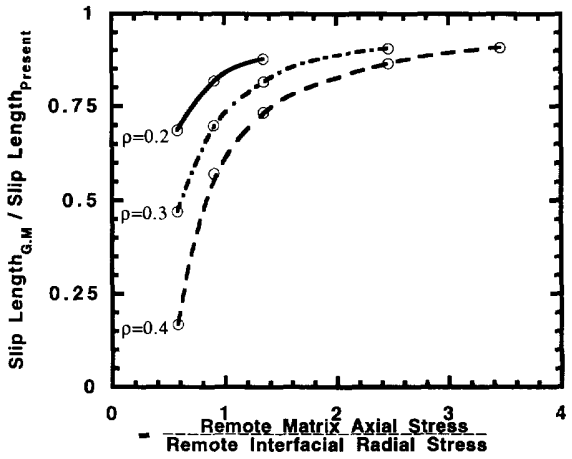

Fig. 4. Ratio of slip length of Gu and Mangonon type of model to the present model as a function of the negative of the ratio of the remote axial matrix stress to the remote interfacial radial stress for constant coefficients of friction.

In Fig. 3, the value of ARS = 1.641 corresponds to zero remote axial strain. It is important to note that, at this value of ARS, a slip zone has already been created at the interface owing to the residual stresses.

The slip lengths obtained from this model are compared with those obtained by using an equivalent Gu and Mangonon (1992) type of model. The equivalent Gu and Mangonon (1992) model is developed by using the same boundary conditions and thermomechanical loads as those given in this paper. The assumptions that are different in their model are:

(i) The axial stresses (σ_{zz}) in the fiber and the matrix are independent of the radial coordinate;
(ii) the stick zone condition of continuous axial displacements, eqn (2i), is replaced by a shear and normal stress relationship:

$$\sigma^0_{rz}(r, z) = -\rho^* \sigma^0_{rr}(r, z), \quad z_2 < z < \infty, \tag{39}$$

where

$$\rho^* = \rho e^{(z_2 - z)/a} \tag{40}$$

and ρ^* is called the "fictitious" coefficient of friction. Equations (39) and (40) satisfy the continuity of shear and radial traction at the slip–stick transition point, $z = z_2$. It also satisfies the condition of vanishing shear stresses as $z \to \infty$.

Figure 4 shows the ratio of the slip lengths obtained from Gu and Mangonon's (1992) type of model and the present model as a function of the stress ratio, ARS, for constant coefficients of friction. The ratio of the two slip lengths approaches unity as ARS increases, which may be an indication that, for large slip lengths, the predictions from the two models are the same.

The following properties are additionally assumed in order to discuss the results in Figs 5–10;

$\alpha_0 = 3.5 \times 10^{-6}$ m/m/°C,
$\alpha_1 = 6.5 \times 10^{-6}$ m/m/°C,
$\Delta T = -1000$°C.

The main assumption in Gu and Mangonon's (1992) model is that the axial stresses

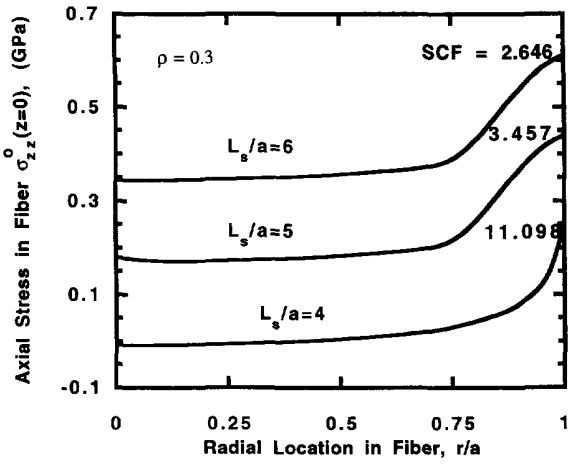

Fig. 5. Fiber axial stresses at the crack plane as a function of the radial location for constant slip lengths.

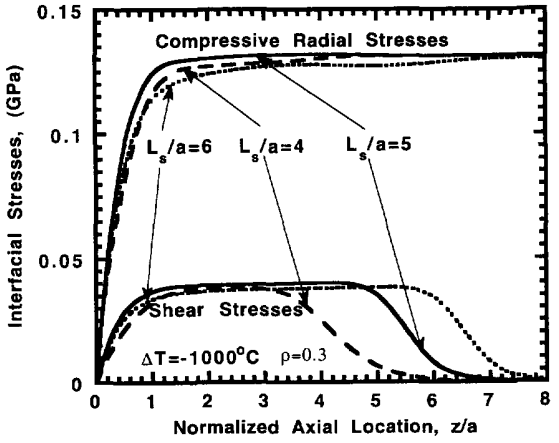

Fig. 6. Interfacial radial and shear stresses as a function of the normalized axial location for constant slip lengths.

(σ_{zz}) are independent of the radial co-ordinate. However, if one looks at Fig. 5, where the fiber axial stresses at the crack plane ($z = 0$) are plotted as a function of the normalized radial co-ordinate, r/a, one can see that this assumption is not valid. The stresses, however, remain fairly constant far away from the interface and far away from the crack plane. One may point out that, as the slip length increases, the stress concentration factor in the fiber, SCF, defined as

$$\text{SCF} = M_4^0(a-,0)/\sigma_{zz}^{0F}(r,\infty), \tag{41}$$

decreases and may be an indication that, for large slip lengths, Gu and Mangonon's (1992) model and the present model give similar results.

In Fig. 6, the interfacial compressive radial and shear stresses are plotted as a function of the normalized axial location, z/a, for constant slip lengths (or constant remote axial strain). The radial stress increases rapidly to the remote radial stress at the interface. Note the small effect of the increasing slip length (increasing remote strain) on the interfacial radial stresses.

The interfacial shear stress in the slip zone follows the same pattern as the interfacial radial stress, since they are linearly related in the slip zone. At the end of the slip zone, the shear stress decays rapidly to zero. Note that the maximum interfacial shear stress is insensitive to increasing slip length (increasing remote strain).

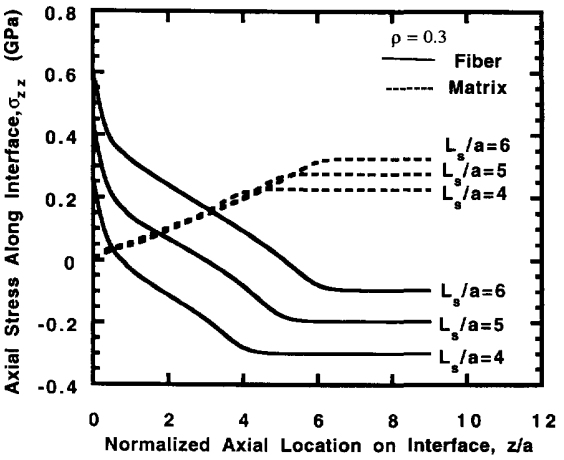

Fig. 7. Interfacial axial stresses as a function of the normalized axial location for constant slip lengths.

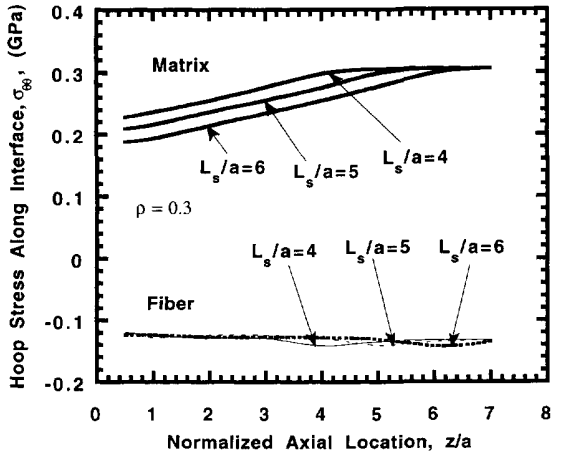

Fig. 8. Interfacial hoop stresses as a function of the normalized axial location for constant slip lengths.

The results from Fig. 6 for $\rho = 0.3$ and for other low friction coefficients (not shown here) make the assumption of constant shear stress for a low friction coefficient used in other models (Wijeyewickrema and Keer, 1993) reasonable. However, one should note that a constant shear stress assumption gives logarithmically singular fiber axial stresses at the crack tip ($r = a, z = 0$) (Wijeyewickrema and Keer, 1993), whereas the Coulomb friction law gives large but finite fiber axial stresses at the crack tip (Schweitert and Steif, 1991).

Figure 7 shows the axial stresses along the fiber and the matrix sides of the interface as a function of the normalized axial location for constant slip lengths. The axial stresses in the fiber are tensile near $z = 0$ (the crack plane) and then become compressive for higher z/a values, reaching the value of the remote axial stresses. Note that these stresses include the contribution from temperature change. The fiber axial stresses are greater as the slip length (remote axial strain) increases, which is expected. The matrix axial stresses start at zero in the crack plane and reach the value of the remote axial stresses at the end of the slip zone. Hence it is important to realize that the sliding interface response to the initial matrix crack does not tend to promote additional matrix cracks by assuming a maximum tensile stress failure criterion for the matrix. However, this does not preclude the appearance of random sites of matrix cracking.

Figure 8 shows the hoop stresses along the interface as a function of the normalized axial location, z/a, for constant slip lengths. The hoop stresses in the fiber along the interface are compressive and almost constant. The effect of slip length (remote axial strain) is very

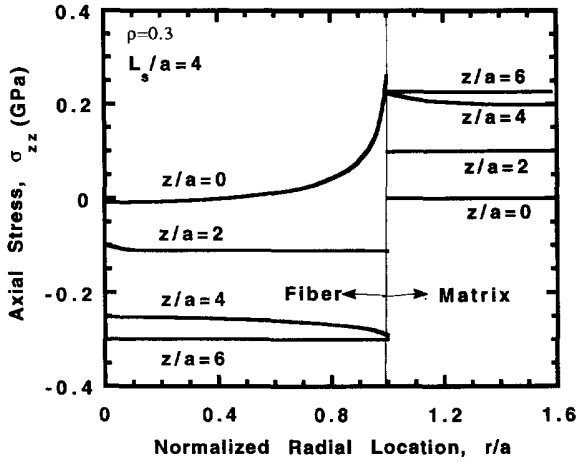

Fig. 9. Fiber and matrix axial stresses as a function of the normalized radial location for constant normalized axial locations.

small on the hoop stresses in the fiber. The hoop stresses in the matrix are tensile and increase away from the transverse crack plane until they reach a constant value that equals the value of the remote hoop stresses. For larger slip lengths, the matrix hoop stresses increase in magnitude and reach the constant value of the remote matrix hoop stresses rapidly.

In Fig. 6 and Fig. 8, the radial and hoop stresses at the interface approach the remote stress values irrespective of the (finite) slip length (or remote axial strain). This is because the radial and the hoop stresses due to the remote axial strain in the uncracked composite cylinder are zero when the Poisson's ratio of the fiber and matrix are equal (Appendix B). The remote hoop and radial stresses are thus only dependent on the constant temperature change, ΔT.

In Fig. 9, the axial stresses in the fiber and matrix are plotted as a function of the normalized radial location for constant values of z in the composite cylinder with a normalized slip length of $L_s/a = 4$. The axial stresses in the fiber and the matrix become nearly independent of the radial co-ordinate away from the crack plane. At $z/a = 6$, the axial stresses are nearly equal to the remote axial stresses. It is also important to note that, for $z/a = 4$, the axial stresses are not constant in both the fiber and the matrix. This again reinforces the conclusion from Fig. 4 that the assumption of radially independent axial stresses made by Gu and Mangonon (1992) is valid only away from the crack plane and the slip–stick transition zone.

Figure 10 shows the normalized opening-crack displacement profiles as a function of the normalized radial location in the matrix, r/a, for constant slip lengths. The curves start at the value of the axial displacement at the interface and increase rapidly to a constant value.

CONCLUSIONS

The following observations are made for the SiC/CAS material system with a frictional fiber–matrix interface under thermomechanical loading, in which the critical assumption that $\alpha_m > \alpha_f$ has been made. The Poisson's ratio of the fiber and the matrix have also been assumed to be equal, and the stick zone is assumed to be of infinite length.

1. The length of the slip zone is a linearly increasing function of the remote mechanical load and a linearly decreasing function of the coefficient of friction. The length of the slip zone is dependent only on the non-dimensional parameter of the ratio between the remote matrix axial stress and the remote radial stress at the interface. Different combinations of temperature difference, remote axial strain, and linear coefficients of

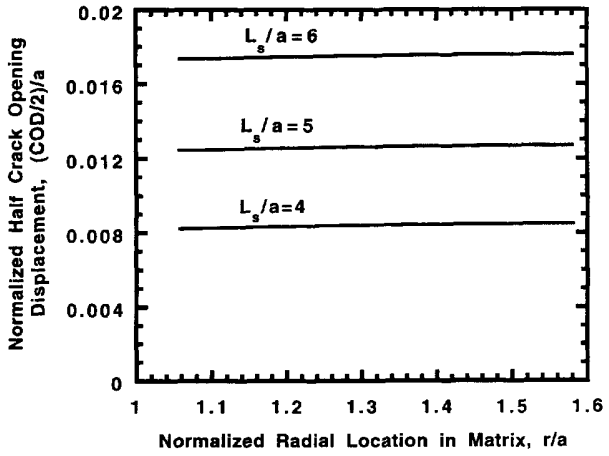

Fig. 10. Normalized crack opening displacements as a function of the normalized radial location for constant slip lengths.

thermal expansion of the fiber and the matrix may result in the same value of the above-mentioned non-dimensional parameter.

2. The axial stresses in the fiber and matrix are fairly independent of the radial coordinate away from the transverse crack plane and the slip–stick transition zone.
3. Only for large slip lengths are the predicted lengths of the slip zone similar in the present model and the shear-lag analysis type of model of Gu and Mangonon (1992).
4. The shear and the radial stresses in the slip zones are fairly constant for low coefficients of friction and may validate models assuming constant shear stress in these cases. These stresses are also nearly independent of the remote mechanical load.
5. The maximum tensile axial and hoop stresses in the matrix are equal to the respective axial and hoop stresses in the uncracked composite cylinder. Hence it is important to realize that the sliding interface response to the initial matrix crack does not tend to promote additional matrix cracks if a maximum tensile stress failure criterion is assumed for the matrix. However, this does not preclude the appearance of random sites of matrix cracking. One should also note in this regard that the crucial assumption made here is of the purely frictional interface (no intrinsic strength) and an infinitely long stick zone.
6. The crack-opening displacement approaches a constant along the radius away from the interface.

Acknowledgements—This work was supported by AFOSR, Bolling AFB, Washington, DC, USA, via Grant No. F49620-92-J-0542. The support of the AFOSR grant monitor, Dr Walter Jones, is deeply appreciated. The authors also thank two anonymous reviewers for their comments on the original manuscript.

REFERENCES

Abramowitz, M. and Stegun, I. A. (1970). *Handbook of Mathematical Functions*. Dover, New York, NY, USA.

Aksel, B., Hui, C. and Lagoudas, D. C. (1991). Effects of a frictional interface on the load diffusion from a broken filament embedded in an elastic medium. *Int. J. Solids Structures* **27**, 833–847.

Byrd, P. F. and Friedman, M. D. (1971). *Handbook of Elliptic Integrals for Engineers and Scientists*, 2nd edition. Springer-Verlag, New York, NY, USA.

Chawla, K. K. (1987). *Composite Materials*. Springer-Verlag, New York, NY, USA.

Daniel, I. M., Anastassopoulos, G. and Lee, J. W. (1989). Experimental micromechanics of brittle-matrix composites, In *Micromechanics: Experimental Techniques* (Edited by W. N. Sharpe, Jr) (AMD Vol. 102), pp. 133–146. American Society of Mechanical Engineers, New York, NY, USA.

Davis, P. J. and Rabinowitz, P. (1984). *Methods of Numerical Integration*. Academic Press, New York, NY, USA.

Dundurs, J. and Comninou, M. (1979). Some consequences of the inequality conditions in contact and crack problems, *J. Elasticity* **9**, 71–82.

Gradshetyn, I. S. and Ryzhik, I. M. (1988). *Tables of Integrals, Series and Products*. Academic Press, New York, NY, USA.

Gu, L. and Mangonon, P. L. (1992). Mechanical characteristics of fiber-reinforced brittle matrix composite. Case II: Non-zero radial stress at matrix external surface. In *Constitutive Behavior of High-temperature Composites* (MD-Vol 40), pp. 151–161. American Society of Mechanical Engineers, New York, NY, USA.

Gupta, G. D. (1973). A layered composite with a broken laminate. *Int. J. Solids Structures* **9,** 1141–1154.
Hseuh, C. and Becher, P. F. (1988). Thermal expansion coefficients of unidirectional fiber-reinforced ceramics. *J. Am. Ceram. Soc.* **71,** C438–C441.
Hseuh, C. and Becher, P. F. (1989). Correction to thermal expansion coefficients of unidirectional fiber-reinforced ceramics. *J. Am. Ceram. Soc.* **72,** 359.
IMSL (1987). *IMSL FORTRAN Subroutines for Mathematical Applications, Math/Library, Version* 1.0. IMSL, Dallas, TX, USA.
Kaw, A. K. and Pagano, N. J. (1993). Axisymmetric thermoelastic response of a composite cylinder containing an annular matrix crack. *J. Compos. Mater.* **27,** 540–571.
Lu, M. and Erdogan, F. (1984). Stress intensity factors in two bonded elastic layers containing cracks perpendicular to and on the interface. *Engng Fract. Mech.* **18,** 491–506.
MACSYMA Reference Manual (1985), Version 11, Symbolics, Boston, MA, USA.
Pagano, N. J. and Brown, H. W., III (1993). The full-cell cracking mode in unidirectional brittle matrix composites. *Composites* **24,** 69–83.
Steif, P. S. (1984). Stiffness reduction due to fiber breakage. *J. Compos. Mater.* **18,** 153–172.
Schweitert, H. R. and Steif, P. S. (1991). Analysis of a broken fiber in a weakly bonded composite. *Int. J. Solids Structures* **28,** 283–297.
Wijeyewickrema, A. C. and Keer, L. M. (1993). Matrix cracking in a fiber reinforced composite with slip at the fiber–matrix interface. *Int. J. Solids Structures* **30,** 91–113.
Zak, A. R. (1972). Elastic analysis of cylindrical configurations with stress singularities. *ASME J. Appl. Mech.* **39,** 501–506.

APPENDIX A

Uncracked stress field for fiber and matrix under thermal loading for a perfect interfacial bond

The stress field for a composite cylinder in a state of generalized plane strain (ε_z = constant) under a temperature change ΔT only is given by (Hseuh and Becher, 1988, 1989)

$$\sigma_{rr}^{0T}(r,z) = AB, \tag{A1}$$

$$\sigma_{\theta\theta}^{0T}(r,z) = AB, \tag{A2}$$

$$\sigma_{zz}^{0T}(r,z) = AC, \tag{A3}$$

$$\sigma_{rz}^{0T}(r,z) = 0, \tag{A4}$$

$$u_r^{0T}(r,z) = \frac{r}{E_0}[\sigma_{\theta\theta}^{0T}(r,z) - v_0(\sigma_{rr}^{0T}(r,z) + \sigma_{zz}^{0T}(r,z))] + r\alpha_0\Delta T, \tag{A5}$$

$$u_z^{0T}(r,z) = \frac{z}{E_0}[\sigma_{zz}^{0T}(r,z) - v_0(\sigma_{rr}^{0T}(r,z) + \sigma_{\theta\theta}^{0T}(r,z))] + z\alpha_0\Delta T, \tag{A6}$$

$$\sigma_{rr}^{1T}(r,z) = \frac{a^2(c^2-r^2)AB}{r^2(c^2-a^2)}, \tag{A7}$$

$$\sigma_{\theta\theta}^{1T}(r,z) = -\frac{a^2(c^2+r^2)AB}{r^2(c^2-a^2)}, \tag{A8}$$

$$\sigma_{zz}^{1T}(r,z) = -\frac{f}{1-f}AC, \tag{A9}$$

$$\sigma_{rz}^{1T}(r,z) = 0, \tag{A10}$$

$$u_r^{1T}(r,z) = \frac{r}{E_1}[\sigma_{\theta\theta}^{1T}(r,z) - v_1(\sigma_{rr}^{1T}(r,z) + \sigma_{zz}^{1T}(r,z))] + r\alpha_1\Delta T, \tag{A11}$$

$$u_z^{1T}(r,z) = \frac{z}{E_1}[\sigma_{zz}^{1T}(r,z) - v_1(\sigma_{rr}^{1T}(r,z) + \sigma_{\theta\theta}^{1T}(r,z))] + z\alpha_1\Delta T, \tag{A12}$$

where

$$A = 1\Big/\left\{\frac{(1+v_0)(1-2v_0)}{E_0^2} + \frac{f(2-v_0-v_1-4v_0v_1)+1+v_1}{(1-f)E_0E_1} + \frac{f(1+v_1)(1+f-2fv_1)}{(1-f)^2E_1^2}\right\}, \tag{A13}$$

$$B = \left[\left(\frac{(1+v_0)}{E_0} + \frac{f}{(1-f)}\cdot\frac{1+v_1}{E_1}\right)\alpha_1 - \left(\frac{1}{E_0} + \frac{f}{1-f}\cdot\frac{1}{E_1}\right)\alpha_0 - \left(\frac{v_0}{E_0} + \frac{f}{1-f}\cdot\frac{v_1}{E_1}\right)\alpha_0\right]\Delta T, \tag{A14}$$

$$C = \left[\left(\frac{(1+\nu_0)}{E_0} + \frac{1+f}{1-f}\cdot\frac{1+\nu_1}{E_1}\right)\alpha_1 - 2\left(\frac{\nu_0}{E_0} + \frac{f}{1-f}\cdot\frac{\nu_1}{E_1}\right)\alpha_0 - \left\{\frac{1-\nu_0}{E_0} + \frac{1}{E_1}\left(\frac{1+f}{1-f} + \nu_1\right)\right\}\alpha_0\right]\Delta T, \quad \text{(A15)}$$

f = fiber volume ratio (a^2/c^2),
α_1 = thermal expansion coefficient of matrix,
α_0 = thermal expansion coefficient of the fiber.

APPENDIX B

Uncracked stress field for fiber and matrix under uniform axial strain for a perfect interfacial bond

The stress field for a composite cylinder in a state of generalized plane strain subjected to a uniform remote axial strain ε_0 (Chawla, 1987) is

$$\sigma_{rr}^{0c}(r,z) = -A', \quad \text{(B1)}$$

$$\sigma_{\theta\theta}^{0c}(r,z) = -A', \quad \text{(B2)}$$

$$\sigma_{zz}^{0c}(r,z) = E_0\varepsilon_0 - 2\nu_0 A', \quad \text{(B3)}$$

$$\sigma_{rz}^{0c}(r,z) = 0, \quad \text{(B4)}$$

$$u_r^{0c}(r,z) = \frac{r}{E_0}[\sigma_{\theta\theta}^{0c}(r,z) - \nu_0(\sigma_{rr}^{0c}(r,z) + \sigma_{zz}^{0c}(r,z))], \quad \text{(B5)}$$

$$u_z^{0c}(r,z) = \varepsilon_0 z, \quad \text{(B6)}$$

$$\sigma_{rr}^{1c}(r,z) = \frac{a^2}{c^2-a^2}\left(1 - \frac{c^2}{r^2}\right)A', \quad \text{(B7)}$$

$$\sigma_{\theta\theta}^{1c}(r,z) = \frac{a^2}{c^2-a^2}\left(1 + \frac{c^2}{r^2}\right)A', \quad \text{(B8)}$$

$$\sigma_{zz}^{1c}(r,z) = E_1\varepsilon_0 + 2\nu_1 A'\frac{a^2}{c^2-a^2}, \quad \text{(B9)}$$

$$\sigma_{rz}^{1c}(r,z) = 0, \quad \text{(B10)}$$

$$u_r^{1c}(r,z) = \frac{r}{E_1}[\sigma_{\theta\theta}^{1c}(r,z) - \nu_1\{\sigma_{rr}^{1c}(r,z) + \sigma_{zz}^{1c}(r,z)\}], \quad \text{(B11)}$$

$$u_z^{1c}(r,z) = \varepsilon_0 z, \quad \text{(B12)}$$

where

$$A' = \frac{2\varepsilon_0 V_1(\nu_1 - \nu_0)}{V_0/k_{p1} + V_1/k_{p0} + 1/\mu_1}, \quad \text{(B13)}$$

$$k_{p0} = \frac{E_0}{2(1+\nu_0)(1-2\nu_0)}, \quad \text{(B14)}$$

$$k_{p1} = \frac{E_1}{2(1+\nu_1)(1-2\nu_1)}, \quad \text{(B15)}$$

$$V_0 = 1 - V_1 = \frac{a^2}{c^2}. \quad \text{(B16)}$$

APPENDIX C

Integrands in integral expressions for the displacements and stresses in solid and hollow cylinders

The expressions for k_{1i} and k_{2i} in eqn (9) are given by

$$k_{li} = \sum_{j=1}^{2} E_{ij}(r,s)f_{jl}(s), \quad l = 1,2 \quad \text{and} \quad i = 1,2,3,4,5, \quad \text{(C1)}$$

$$\alpha_{ij}f_{jl} = \gamma_{il}, \quad j = 1,2, \quad i = 1,2 \quad \text{and} \quad l = 1,2. \quad \text{(C2)}$$

$$\alpha_{11} = \bar{I}_1(as),$$
$$\alpha_{12} = as\bar{I}_0(as) + 2(1-\nu_0)\bar{I}_1(as),$$
$$\alpha_{21} = -\bar{I}_0(as) + \bar{I}_1(as)/(as),$$
$$\alpha_{22} = (2\nu_0 - 1)\bar{I}_0(as) - (as)\bar{I}_1(as), \tag{C3}$$

$$\gamma_{11} = \gamma_{22} = \frac{1}{s^3}, \quad \gamma_{12} = \gamma_{21} = 0, \tag{C4}$$

$$E_{11} = -\frac{1}{2\mu_0}s^2\bar{I}_1(rs)\,e^{-(a-r)s}, \quad E_{12} = -\frac{1}{2\mu_0}s^2 rs\bar{I}_0(rs)\,e^{-(a-r)s},$$
$$E_{21} = \frac{1}{2\mu_0}s^2\bar{I}_0(rs)\,e^{-(a-r)s}, \quad E_{22} = \frac{1}{2\mu_0}s^2[4(1-\nu_0)\bar{I}_0(rs) + rs\bar{I}_1(rs)]\,e^{-(a-r)s},$$
$$E_{31} = s^3[-\bar{I}_0(rs) + \bar{I}_1(rs)/(rs)]\,e^{-(a-r)s}, \quad E_{32} = s^3[(2\nu_0 - 1)\bar{I}_0(rs) - rs\bar{I}_1(rs)]\,e^{-(a-r)s},$$
$$E_{41} = s^3\bar{I}_0(rs)\,e^{-(a-r)s}, \quad E_{42} = s^3[2(2-\nu_0)\bar{I}_0(rs) + rs\bar{I}_1(rs)]\,e^{-(a-r)s},$$
$$E_{51} = s^3\bar{I}_1(rs)\,e^{-(a-r)s}, \quad E_{52} = s^3[rs\bar{I}_0(rs) + 2(1-\nu_0)\bar{I}_1(rs)]\,e^{-(a-r)s}, \tag{C5}$$

$$\bar{I}_i(x) = e^{-x}I_i(x), \tag{C6}$$

where $I_i(x)$, $i = 0,1$, is the hyperbolic Bessel's function.

The above expressions have been obtained by solving the boundary value problem with boundary conditions given by using Love's stress functions (Wijeyewickrema and Keer, 1991), defined for the axisymmetric torsionless infinite solid cylinder. The reason for writing the expressions in the form of eqn (9) is that one can reduce the double integrals to single integrals by a judicious choice of the unknown traction functions S_0 and T_0, and also by reducing the parameter k_{li}^{∞} as a product of $e^{-(a-r)s}$ and terms of order s^{-1} and higher.

The k_{li}^{∞} terms are evaluated by finding k_{li}^{∞} in closed form as $s \to \infty$ by using the asymptotic expansion for $I_i(x)$ for large values of x as (Abramowitz and Stegun, 1970, p. 377)

$$I_i(x) = \left(1 - \frac{\delta - 1}{8x} + \frac{(\delta-1)(\delta-9)}{2(8x)^2} - \cdots\right)\frac{e^x}{\sqrt{2\pi x}}, \quad i = 0, 1, 2, \quad \delta = 4i^2. \tag{C7}$$

The expressions for p_{1i}, p_{2i}, and p_{3i} in eqn (11) are given by

$$k_{li} = \sum_{j=1}^{2} E_{ij}(r,s)f_{jl}(s), \quad l = 1,2 \quad \text{and} \quad i = 1,2,3,4,5, \tag{C8}$$

$$\alpha_{ij}f_{jl} = \gamma_{il}, \quad j = 1,2, \quad i = 1,2 \quad \text{and} \quad l = 1,2. \tag{C9}$$

$$\alpha_{11} = \bar{I}_1(as)$$
$$\alpha_{12} = as\bar{I}_0(as) + 2(1-\nu_0)\bar{I}_1(as)$$
$$\alpha_{21} = -\bar{I}_0(as) + \bar{I}_1(as)/(as)$$
$$\alpha_{22} = (2\nu_0 - 1)\bar{I}_0(as) - (as)\bar{I}_1(as) \tag{C10}$$

$$\gamma_{11} = \gamma_{22} = \frac{1}{s^3}, \quad \gamma_{12} = \gamma_{21} = 0, \tag{C11}$$

$$E_{11} = -\frac{1}{2\mu_0}s^2\bar{I}_1(rs)\,e^{-(a-r)s}, \quad E_{12} = -\frac{1}{2\mu_0}s^2 rs\bar{I}_0(rs)\,e^{-(a-r)s},$$
$$E_{21} = \frac{1}{2\mu_0}s^2\bar{I}_0(rs)\,e^{-(a-r)s}, \quad E_{22} = \frac{1}{2\mu_0}s^2[4(1-\nu_0)\bar{I}_0(rs) + rs\bar{I}_1(rs)]\,e^{-(a-r)s},$$
$$E_{31} = s^3[-\bar{I}_0(rs) + \bar{I}_1(rs)/(rs)]\,e^{-(a-r)s}, \quad E_{32} = s^3[(2\nu_0 - 1)\bar{I}_0(rs) - rs\bar{I}_1(rs)]\,e^{-(a-r)s},$$
$$E_{41} = s^3\bar{I}_0(rs)\,e^{-(a-r)s}, \quad E_{42} = s^3[2(2-\nu_0)\bar{I}_0(rs) + rs\bar{I}_1(rs)]\,e^{-(a-r)s},$$
$$E_{51} = s^3\bar{I}_1(rs)\,e^{-(a-r)s}, \quad E_{52} = s^3[rs\bar{I}_0(rs) + 2(1-\nu_0)\bar{I}_1(rs)]\,e^{-(a-r)s}, \tag{C12}$$

$$\bar{I}_i(x) = e^{-x}I_i(x). \tag{C13}$$

$$p_{li} = \sum_{j=1}^{4} F_{ij}(r,s)\,g_{jl}(s), \quad l = 1,2,3 \quad \text{and} \quad i = 1,2,3,4,5,6, \tag{C14}$$

$$\beta_{ij}g_{jl} = \Gamma_{il}, \quad j = 1,2,3,4, \quad i = 1,2,3,4, \quad \text{and} \quad l = 1,2,3. \tag{C15}$$

$$\left.\begin{aligned}
&\Gamma_{11} = \Gamma_{22} = \frac{1}{s^3}, \\
&\Gamma_{ij} = 0, \quad j = 1, 2, \quad i = 1, 2, 3, 4, \quad i \neq j, \\
&\Gamma_{i3} = \frac{h_i(s,t)}{s^3}, \quad i = 1, 2, 3, 4.
\end{aligned}\right\} \tag{C16}$$

$$\begin{aligned}
\beta_{11} &= \overline{I_1}(bs)\,e^{-(c-b)s}, \\
\beta_{12} &= [bs\overline{I_0}(bs) + 2(1-\nu_1)\overline{I_1}(bs)]\,e^{-(c-b)s}, \\
\beta_{13} &= -\overline{K_1}(bs), \\
\beta_{14} &= -bs\overline{K_0}(bs) + 2(1-\nu_1)\overline{K_1}(bs), \\
\beta_{21} &= [-\overline{I_0}(bs) + \overline{I_1}(bs)/(bs)]\,e^{-(c-b)s}, \\
\beta_{22} &= -[(1-2\nu_1)\overline{I_0}(bs) + bs\overline{I_1}(bs)]\,e^{-(c-b)s}, \\
\beta_{23} &= -[\overline{K_0}(bs) + \overline{K_1}(bs)/(bs)], \\
\beta_{24} &= (1-2\nu_1)\overline{K_0}(bs) - bs\overline{K_1}(bs), \\
\beta_{31} &= -\overline{I_1}(cs), \\
\beta_{32} &= -cs\overline{I_0}(cs), \\
\beta_{33} &= \overline{K_1}(cs)\,e^{-(c-b)s}, \\
\beta_{34} &= cs\overline{K_0}(cs)\,e^{-(c-b)s}, \\
\beta_{41} &= \overline{I_1}(cs), \\
\beta_{42} &= cs\overline{I_0}(cs) + 2(1-\nu_1)\overline{I_1}(cs), \\
\beta_{43} &= -\overline{K_1}(cs)\,e^{-(c-b)s}, \\
\beta_{44} &= [-cs\overline{K_0}(cs) + 2(1-\nu_1)\overline{K_1}(cs)]\,e^{-(c-b)s}.
\end{aligned} \tag{C17}$$

$$\begin{aligned}
F_{11} &= -\tfrac{1}{2}\mu_1\overline{I_1}(rs)\,e^{-s(c-r)}, \\
F_{12} &= rs\overline{I_0}(rs)\,e^{-s(c-r)}, \\
F_{13} &= \overline{K_1}(rs)\,e^{s(b-r)}, \\
F_{14} &= rs\overline{K_0}(rs)s^2\,e^{s(b-r)}, \\
F_{21} &= \tfrac{1}{2}\mu_1\overline{I_0}(rs)\,e^{-s(c-r)}, \\
F_{22} &= [4(1-\nu_1)\overline{I_0}(rs) + rs\overline{I_1}(rs)]\,e^{-s(c-r)}, \\
F_{23} &= \overline{K_0}(rs)\,e^{s(b-r)}, \\
F_{24} &= [rs\overline{K_1}(rs) - 4(1-\nu_1)\overline{K_0}(rs)]\,e^{s(b-r)}, \\
F_{31} &= [-\overline{I_0}(rs) + \overline{I_1}(rs)/(rs)]\,e^{-s(c-r)}, \\
F_{32} &= [(2\mu_0 - 1)\overline{I_0}(rs) - rs\overline{I_1}(rs)]\,e^{-s(c-r)}, \\
F_{33} &= [\overline{K_0}(rs) + \overline{K_1}(rs)/(rs)]\,e^{s(b-r)}, \\
F_{34} &= [(1-2\nu_1)\overline{K_0}(rs) - rs\overline{K_1}(rs)]\,e^{s(b-r)}, \\
F_{41} &= \overline{I_0}(rs)\,e^{-s(c-r)}, \\
F_{42} &= [2(2-\nu_1)\overline{I_0}(rs) + rs\overline{I_1}(rs)]\,e^{-s(c-r)}, \\
F_{43} &= \overline{K_0}(rs)\,e^{s(b-r)}, \\
F_{44} &= [-2(2-\nu_1)\overline{K_0}(rs) + rs\overline{K_1}(rs)]\,e^{s(b-r)}, \\
F_{51} &= \overline{I_1}(rs)\,e^{-s(c-r)}, \\
F_{52} &= [rs\overline{I_0}(rs) + 2(1-\nu_1)\overline{I_1}(rs)]\,e^{-s(c-r)}, \\
F_{53} &= \overline{K_1}(rs)\,e^{s(b-r)}, \\
F_{54} &= [2(1-\mu_1)\overline{K_1}(rs) - rs\overline{K_0}(rs)]\,e^{s(b-r)}, \\
F_{6j} &= \frac{2\mu_1(1-\nu_1)}{r}F_{ij} + \nu_1(F_{3j} + F_{4j}), \quad j = 1, 2, 3, 4,
\end{aligned} \tag{C18}$$

$$\overline{K_i}(x) = e^{x} K_i(x), \tag{C19}$$

where $K_i(x)$, $i = 0, 1$ are the Bessel's functions of the second kind.

$$\phi(r) = \frac{\mu_1}{1-\nu_1}\frac{\partial \hat{c}}{\partial r} M_2(r, 0), \quad d < r < e, \tag{C20}$$

$$\begin{aligned}
h_1(t,s) &= -s[bsI_0(bs)K_1(ts) - tsI_1(bs)K_0(ts)]\, e^{-(t-b)s},\\
h_2(t,s) &= -s\left[tsI_0(bs)K_0(ts) + I_0(bs)K_1(ts) - \frac{t}{b}I_1(bs)K_0(ts) - \left[bs + \frac{2(1-\nu_1)}{bs}\right]I_1(bs)K_1(ts)\right]e^{-(t-b)s},\\
h_3(t,s) &= -s[-tsI_0(ts)K_1(cs) + csI_1(ts)K_0(cs) + 2(1-\nu_1)I_1(ts)K_1(cs)]\, e^{-(c-t)s},\\
h_4(t,s) &= -s[-tsI_0(ts)K_1(cs) - csI_1(ts)K_0(cs)]\, e^{-(c-t)s},
\end{aligned} \tag{C21}$$

$$\begin{aligned}
N_1(r,t,z) &= t[(1-2\nu_1)I_{01} - zI_{11}],\\
N_2(r,t,z) &= t[2(1-\nu_1)I_{00} + zI_{10}] - \frac{(1-\nu_1)}{\mu_1},\\
N_3(r,t,z) &= t\left[I_{01} - zI_{02} - \frac{(1-2\nu_1)}{r}I_{10} - \frac{z}{r}I_{11}\right],\\
N_4(r,t,z) &= t[I_{01} + zI_{02}], \quad z > 0,\\
&= \frac{m(r,t)-1}{t-r} + \frac{m(r,t)}{t+r}, \quad z = 0,\\
m(r,t) &= E\left(\frac{r}{t}\right), \quad r < t,\\
&= \frac{r}{t}E\left(\frac{t}{r}\right) + \frac{t^2-r^2}{rt}K\left(\frac{t}{r}\right), \quad r > t,\\
N_5(r,t,z) &= tzI_{12},\\
N_6(r,t,z) &= t\left[\frac{(1-2\nu_1)}{r}I_{10} - \frac{z}{r}I_{11} + 2\nu_1\right],
\end{aligned} \tag{C22}$$

$$I_{ij} = \int_0^{\infty} p^j e^{-zp} J_1(pt) J_i(rp)\, dp. \tag{C23}$$

Equation (11) was obtained by using the expression given for stresses and displacements in an infinite isotropic hollow cylinder (Erdol and Erdogan, 1978) and applying the boundary conditions given by eqn (10). The integrals in eqn (C23) can be simplified in terms of the elliptic integrals of the first, second, and third kinds. The parameters p_{ij}^{∞} are evaluated by finding p_{ij} as $s \to \infty$ by using the asymptotic expansion for $I_i(x)$ as given by eqn (C14) and $K_i(x)$ for large values of x as (Abramowitz and Stegun, 1970, p. 377):

$$K_i(x) = \left(1 + \frac{\delta-1}{8x} + \frac{(\delta-1)(\delta-9)}{2(8x)^2} + \cdots\right)\frac{e^{-x}}{\sqrt{2\pi x}}, \quad i = 0, 1, \quad \delta = 4i^2. \tag{C24}$$

The parameters $p_{3i}^{b\infty}$ and $p_{3i}^{c\infty}$ are asymptotic values of $p_{3i}(r, s \to \infty)$ as $r \to b$ and $r \to c$, respectively.

APPENDIX D

Formulas used for the stresses in the fiber and matrix due to crack

From Abramowitz and Stegun (1970, pp. 709, 907) and Gradshetyn and Ryzhik (1965, p. 590), we have

$$\int_0^{\infty} p^m e^{-zp} J_1(rp) J_1(pt)\, dp = (-1)^m \frac{d^m}{dz^m}\frac{1}{\pi\sqrt{rt}} Q_{1/2}(w), \quad m \geqslant 0, \tag{D1}$$

$$\int_0^{\infty} p^m e^{-zp} J_0(rp) J_1(pt)\, dp = (-1)^{m-1}\frac{d}{dt}\left[\frac{d^{m-1}}{dz^{m-1}}\frac{1}{\pi\sqrt{rt}} Q_{-1/2}(w)\right], \quad m \geqslant 1, \tag{D2}$$

where $Q_\nu(w)$ is the associated Legendre function,

$$w = \frac{z^2 + r^2 + t^2}{2rt}, \tag{D3}$$

$$Q_{1/2}(w) = wyK(y) - \frac{2}{y}E(y), \tag{D4}$$

$$Q_{-1/2}(w) = yK(y), \tag{D5}$$

$$y = [2/(1+w)]^{1/2}, \tag{D6}$$

$$\frac{dK(y)}{dy} = \frac{E(y)}{y(1-y^2)} - \frac{K(y)}{y}, \tag{D7}$$

$$\frac{dE(y)}{dy} = \frac{E(y) - K(y)}{y}. \tag{D8}$$

$$K(y) = \int_0^{\pi/2} [1 - y^2 \sin^2(\theta)]^{-1/2}\, d\theta, \tag{D9}$$

$$E(y) = \int_0^{\pi/2} [1 - y^2 \sin^2(\theta)]^{1/2}\, d\theta, \tag{D10}$$

where

$K(y)$ is the complete elliptic integral of the first kind, and
$E(y)$ is the complete elliptic integral of the second kind.

The integrals in eqns (D9) and (D10) are evaluated by using the IMSL (1987) routines, DELK and DELE, respectively. Note the difference between the definitions of the elliptic integrals in eqns (D9) and (D10) and that given in the IMSL (1987) manual.

We also have (Byrd and Friedman, 1971, pp. 8, 251)

$$\int_0^\infty e^{-zp} J_0(rp) J_1(pt)\, dp = \frac{1}{\pi - 2}[E(k)F(\beta, k') + K(k)E(\beta, k') - K(k)F(\beta, k)]), \tag{D11}$$

where $F(x, y)$ is the normal elliptic integral of the first kind, and
$E(x, y)$ is the normal elliptic integral of the second kind,

$$F(x, y) = \int_0^x [1 - y^2 \sin^2(\theta)]^{-1/2}\, d\theta, \tag{D12}$$

$$E(x, y) = \int_0^x [1 - y^2 \sin^2(\theta)]^{1/2}\, d\theta, \tag{D13}$$

$$\beta = \sin^{-1}[(1/2(1 + q_2/\sqrt{q_1})]^{1/2}, \tag{D14}$$

$$k'^2 = 1 - k^2, \tag{D15}$$

$$k^2 = ([q_3 + \sqrt{q_1}][q_4 + \sqrt{q_1}])/([q_5 + \sqrt{q_1}][q_6 + \sqrt{q_1}]), \tag{D16}$$

$$q_1 = (z^2 + r^2 + t^2)^2 - 4r^2t^2, \quad q_2 = z^2 + r^2 - t^2, \tag{D17}$$

$$q_3 = t^2 - z^2 - r^2, \quad q_4 = r^2 - z^2 - t^2, \tag{D18}$$

$$q_5 = z^2 + r^2 - t^2, \quad q_6 = z^2 - r^2 + t^2. \tag{D19}$$

The integrals in eqns (D12) and (D13) are evaluated by using the adaptive Simpson's one-third rule.

APPENDIX E

Formulas used to simplify equations (9) and (11)

$$\frac{d^m}{ds^m}\int_a^b \sin(sz)\,dz = \frac{d^m}{ds^m}\left[\frac{\cos(as)-\cos(bs)}{s}\right], \tag{E1}$$

$$\frac{d^m}{ds^m}\int_a^b \cos(sz)\,dz = \frac{d^m}{ds^m}\left[\frac{\sin(bs)-\sin(as)}{s}\right], \tag{E2}$$

$$\int_a^\infty \frac{\sin(sz)\,dz}{z^3} = \frac{\sin(sa)}{2a^2} + \frac{s\cos(sa)}{2a} + \frac{s^2}{2} + si(as), \tag{E3}$$

$$\int_a^\infty \frac{\cos(sz)\,dz}{z^3} = \frac{\cos(sa)}{2a^2} + \frac{s\sin(sa)}{2a} + \frac{s^2}{2} + ci(as), \tag{E4}$$

where

$$si(x) = -\frac{\pi}{2} + \int_0^x \frac{\sin(t)}{t}\,dt, \tag{E5}$$

$$ci(x) = C + \ln(x) + \int_0^x \frac{\cos(t)-1}{t}\,dt, \tag{E6}$$

where $C = 0.577\,215\,664\,901\,532\,860\,606\,512$ (Euler's Constant),

$$\frac{d^n}{da^n}\int_0^\infty e^{-as}\cos(st)\,ds = \frac{d^n}{da^n}\left(\frac{a}{a^2+t^2}\right), \tag{E7}$$

$$\frac{d^n}{da^n}\int_0^\infty e^{-as}\sin(st)\,ds = \frac{d^n}{da^n}\left(\frac{t}{a^2+t^2}\right). \tag{E8}$$

For large values of (as), eqns (E3) and (E4) do not give accurate results. In these cases, Filon's method of integration (Davis and Rabinowitz, 1984, p. 151) was used as follows.

$$\int_a^{b^*} f(t)\cos(kt)\,dt \simeq h\{\alpha[f(b^*)\sin(kb^*) - f(a)\sin(ka)] + \beta C_{2n} + \gamma C_{2n-1}, \tag{E9}$$

$$\int_a^{b^*} f(t)\sin(kt)\,dt \simeq h\{-\alpha[f(b^*)\cos(kb^*) - f(a)\cos(ka)] + \beta S_{2n} + \gamma S_{2n-1}, \tag{E10}$$

$$\alpha = (\theta^2 + \theta\sin(\theta)\cos(\theta) - 2\sin^2(\theta))/\theta^3, \tag{E11}$$

$$\beta = 2[\theta\{1+\cos^2(\theta)\} - 2\sin(\theta)\cos(\theta)]/\theta^3, \tag{E12}$$

$$\gamma = 4\{\sin(\theta) - \theta\cos(\theta)\}/\theta^3, \tag{E13}$$

$$\theta = kh, \tag{E14}$$

$$h = (b^* - a)/(2n), \tag{E15}$$

$$C_{2n} = \tfrac{1}{2}f(a)\cos(ka) + \sum_{i=1}^{n-1} f(a+2ih)\cos\{k(a+2ih)\} + \tfrac{1}{2}f(b)\cos(kb^*), \tag{E16}$$

$$C_{2n-1} = \sum_{i=1}^{n} f\{a+2i-1)h\}\cos[k\{a+(2i-1)h\}], \tag{E17}$$

$$S_{2n} = -\tfrac{1}{2}f(a)\sin(ka) - \tfrac{1}{2}f(b^*)\sin(kb^*) + \sum_{i=1}^{n-1} f(a+2ih)\sin\{k(a+2ih)\}, \tag{E18}$$

$$S_{2n-1} = \sum_{i=1}^{n} f\{a+(2i-1)h\}\sin[k\{a+(2i-1)h\}]. \tag{E19}$$

A value of $b^* = a/\sqrt{|\varepsilon_r|}$ was chosen as the upper limit after taking into consideration the following:

$$\int_a^\infty \frac{1}{t^3}\sin(st)\,dt \leqslant \int_a^\infty \left|\frac{1}{t^3}\right| dt = \frac{1}{2a^2} \tag{E20}$$

$$\int_a^{b^*} \left|\frac{1}{t^3}\right| dt = \frac{1}{2a^2} - \frac{1}{2b^{*2}}. \tag{E21}$$

Thus the maximum relative error $|\varepsilon_r|$ in eqn (E21) is given by

$$|\varepsilon_r| = \frac{a^2}{b^{*2}}. \tag{E22}$$

Thus, for a given relative error of ε_r, the upper limit of integration b^* is given by $b^* = a/\sqrt{\varepsilon_r}$.